Applied Physics Letters

Supersonic needle-jet generation with single cavitation bubbles

Cite as: Appl. Phys. Lett. **118**, 134103 (2021); https://doi.org/10.1063/5.0045705
Submitted: 28 January 2021 • Accepted: 15 March 2021 • Published Online: 01 April 2021

Fabian Reuter and Claus-Dieter Ohl

Applied Physics Letters ARTICLE scitation.org/journal/apl

Supersonic needle-jet generation with single cavitation bubbles

Cite as: Appl. Phys. Lett. **118**, 134103 (2021); doi: 10.1063/5.0045705
Submitted: 28 January 2021 · Accepted: 15 March 2021 ·
Published Online: 1 April 2021 · Publisher error corrected: 19 April 2021

Fabian Reuter[a] and Claus-Dieter Ohl

AFFILIATIONS

Faculty of Natural Sciences, Institute for Physics, Department Soft Matter, Otto-von-Guericke University Magdeburg, 39106 Magdeburg, Germany

[a]Author to whom correspondence should be addressed: fabian.reuter@ovgu.de

ABSTRACT

Collapsing cavitation bubbles produce intense microscopic flows. Here, in an aqueous environment, we seed single laser-induced bubbles (diameter about one millimeter) in proximity to a solid surface, in a regime that has not been well explored before in order to generate a "needle jet." The needle jet propagates at supersonic speed through the gas phase toward the solid. It reaches average velocities of more than 850 ms^{-1} and thus is an order of magnitude faster than the regular jets that have frequently been observed in cavitation bubbles. The dynamics leading to the needle jet formation are studied with high speed imaging at five million frames per second with femtosecond illumination. This highly repeatable, localized flow phenomenon may be exploited for injection purposes or material processing, and it is expected to generate significantly larger water hammer pressures and may also play a role in cavitation erosion and peening.

Nearly perfect spherical focusing of energy can be achieved during the collapse of a mostly empty bubble, i.e., a cavitation bubble, in a large volume of liquid. Then, the potential energy stored in the liquid is converted to kinetic energy that focuses at the center of the bubble. However, when the bubble dynamics is restricted by a boundary, whether solid, liquid, or gaseous, the spherical focusing of kinetic energy is hindered, resulting in unexpected rich fluid dynamics. In particular, a jet flow along the axis of symmetry can be generated in the last stage of the bubble collapse.[14] For the cavitation bubbles collapsing at rigid boundaries under investigation here, this jet is directed toward the boundary and reaches velocities of 50–100 ms^{-1}. Diameters are roughly 10–30% of the maximum bubble diameter, i.e., a cavitation bubble of 1 mm diameter displays a jet that is about 100–300 μm wide. This jet plays a role in surface cleaning with ultrasonics or single bubbles as it results in high flow velocities at the boundary, implying sufficiently high wall shear rates for a surface to be cleaned.[18,23] In addition, this jet has also been considered one cause of cavitation erosion.[12]

Jetting of single cavitation bubbles can also be exploited in laser-induced forward transfer. This is an additive printing and manufacturing technique involving the collapse of laser-induced bubbles in somewhat confined geometries to dispense and deliver the "ink"-material.[24] There, the collapsing cavity wall is followed by a flow that converges onto the axis of symmetry, and thereby generates an axial jet with front velocities of the order of several ms^{-1}[19] and more,[29] which is a strong function of liquid viscosity. A stable and repeatable ink dispensing demands controlled jetting, which in turn requires intact geometric symmetry and thus a clean seeding of only one bubble, avoiding any fragmentation of bubble or seeding of spurious bubbles with the laser pulse.[11]

More than 50 years of research on jetting from single and well-controlled cavitation bubbles near rigid boundaries were initiated with the seminal works by Benjamin and Ellis[4] and Lauterborn and Bolle.[13] Most of the research so far looked at the fluid dynamics when the bubble is created not in direct proximity but at some further distances from the boundary. The so-called stand-off distance γ of the bubble to the boundary is conveniently non-dimensionalized by the bubble radius at time of maximum expansion, i.e., $\gamma = d/R_{max}$. Interestingly, most research has focused on the bubble collapse at distances of $\gamma > 0.3$. However, it is at the smaller stand-offs where Benjamin and Ellis photographed in their early work of 1966[4] an "odd" bubble shape dynamics and a "filamentary jet" inside the bubble. They estimated a lower boundary of the jet velocity of 35 ms^{-1}, but they could not explain the jet formation or the particular bubble dynamics that lead to its formation. Only recently, for smaller stand-offs, Lechner *et al.* 2019 and 2020[15,16] reported from the axisymmetric volume of fluid simulations on the generation of similar bubble dynamics that lead to the generation of a very fast and thin jet.

In the present letter, we experimentally investigate cavitation bubbles collapsing in direct proximity to a boundary. We create single bubbles by optic cavitation and study them with optical microscopy and short exposure times to capture their jetting dynamics. The single bubbles are seeded in water at adjustable locations at a solid surface using a focused nanosecond laser pulse (frequency-doubled Nd:YAG laser, model Litron nano S with attenuator, wavelength 532 nm, pulse length ≈5 ns). A schematic of the experimental setup is given in Fig. 1. It also depicts the normalized stand-off distance γ, where d is measured as the distance from the plasma spot to the wall [Fig. 1(b)]. The bubble is produced in de-ionized water in a glass container (dimensions $5 \times 5 \times 8\,\mathrm{cm}^3$). For focusing, a long working distance microscope objective is sealed watertight and embedded into the container bottom (Mitutoyo 50×, NA = 0.42, nominal working distance: 20.5 mm). To avoid laser beam absorption at the solid boundary, as this would produce spurious bubbles, the laser is focused in parallel to the boundary, implying some clipping of the laser beam. This, however, does not affect proper bubble generation, which we confirmed for a free bubble (i.e., without boundary) by covering half of the focusing objective aperture. At the focal spot, a laser plasma is produced to seed a single bubble. This effort is needed to control time and location of bubble generation, i.e., the jitter in timing of bubble generation is less than one nanosecond and in the location of the bubble center is less than one micrometer. The lifetime of the bubble T_L is defined as the period from plasma generation to bubble collapse. Close to the focal spot, either a glass or a polished metallic specimen is placed (dimensions about $5 \times 10 \times 1.5\,\mathrm{mm}^3$). The specimens are positioned with a three-axis micrometer stage and act as almost perfectly rigid boundaries, i.e., the bubble dynamics does not depend on the material employed. The bubble shape dynamics is recorded with two high-speed cameras from two perpendicular perspectives [Photron Fastcam Mini AX operated at 130 000 frames per second (fps), exposure time 360 ns, and Shimadzu HPV-X2 operated at 5×10^6 fps]. The slower camera is used to measure the stand-off distance and affirm proper bubble generation, yet here we present only the time series taken with the faster of the two cameras, which is equipped with either a Mitutoyo 5× or a 20× long working distance microscope objective, implying resolutions of 3.56 μm per pixel and 0.89 μm per pixel, respectively. Uncertainties in the measurement of γ depend on the reading accuracy of R_{max} and d, which we take as $\sqrt{2}$ pixels, resulting in a total uncertainty in γ that is less than 0.01 for the small stand-offs investigated here. Exposure times as short as 220 fs are obtained with an expanded pulse train from a femtosecond laser beam that illuminates the scene (Ekspla Femtolux, wavelength 515 nm). The maximum radii of the bubbles presented here lie in the interval 656 μm ± 12%. Even though to certain aspects of the bubble dynamics at small stand-offs viscosity may play a decisive role, within this small-sized interval, we find that scaling purely on inertia, through γ, works well.

Before coming to the needle jet (NJ) phenomenon, we briefly present the well-known jetting of bubbles, here for a γ-value of 0.98, see Fig. 2. The sequence covers 17 μs when the jet is flattening and threading the bubble from the boundary distant (upper) bubble pole as it is flowing along the axis of symmetry toward the boundary. In distinction to the jetting presented below, we call this jet the "regular jet." Its radius at the instance of impact on the boundary can be estimated from the images as ≈125 μm, which is about 22% R_{max}. For the velocity of this regular jet, we measure $v_{RJ} = 73.4\,\mathrm{ms}^{-1}$, which is in the expected range;[16,21] the supplementary material provides technical details on these measurements.

A considerably different bubble dynamics is achieved when the bubble is seeded closer to the solid. Figure 3 shows this dynamics for $\gamma = 0.053$ from three different views. As a side note, this stand-off regime is experimentally more difficult to prepare and thus has hitherto been largely unexplored. Contrary to the previous case where the indentation from the jet is observed in the axial direction, now, the bubble is indented in the radial direction, see the kink in the first two frames of Figs. 3(a) and 3(b). This is the result of a boundary-parallel cylindrical flow that converges on the axis of symmetry. When it hits the axis of symmetry just before the third frame [Fig. 3(a)], a shock wave (SW) is emitted and the liquid is instantaneously accelerated downwards, leading to the ejection of a thin and fast needle jet into the gas phase. This needle jet has in the fourth frame already impacted onto the boundary. A lower bound of the averaged needle jet and its impact velocity is measured as $v_{NJ} > 850\,\mathrm{ms}^{-1}$. For more details of the velocity measurement, see the supplementary material. This value implies a massive acceleration on the liquid of 1×10^9 g, where g is the gravitational acceleration on Earth. This enormous acceleration

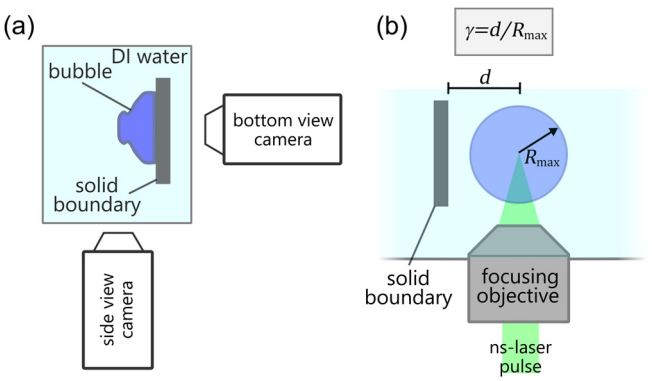

FIG. 1. Experimental setup and geometric definition on the normalized stand-off distance γ. (a) Top view of the water-filled cuvette. The bubble is imaged from two perpendicular perspectives (side view and bottom view) simultaneously. (b) Side view of the setup.

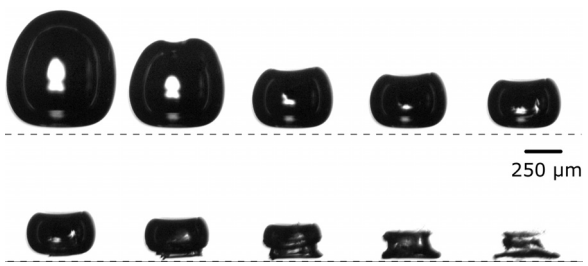

FIG. 2. Time series of a cavitation bubble at a solid surface with regular jetting. The boundary coincides horizontally with the image bottom edge (dashed line). In the second frame, the regular jet, formed above the bubble, is indenting the upper bubble pole. Starting with the third frame, the jet can be observed in the bubble interior. In the sixth frame, the jet has pierced the opposite bubble wall and is impinging onto the boundary. Exposure times are 200 ns, and the frame times are 102, 108, 113, 114, 115, 116, 117, 118, and 119 μs after bubble generation ($\gamma = 0.98$, $R_{max} = 578\,\mu$m, $T_L = 121\,\mu$s).

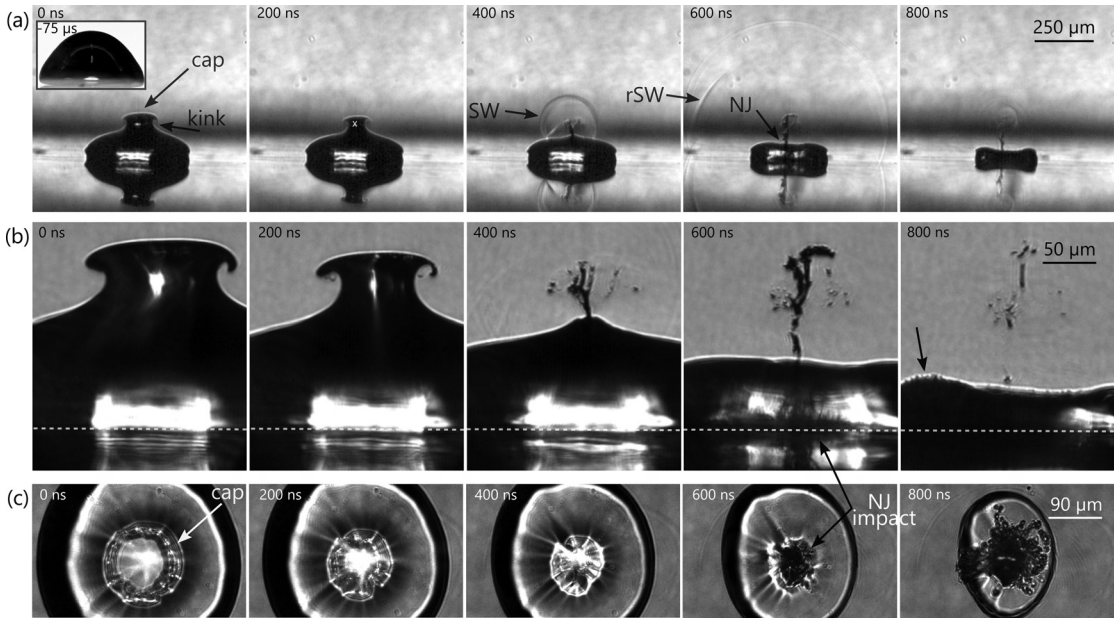

FIG. 3. Three views on the final stage of bubble collapse near a rigid boundary with supersonic needle jet generation at exposure times of 220 fs. Horizontally, subsequent frames are recorded with an interval of 200 ns. Vertically, the frames are aligned to match the same stage of the bubble dynamics. (a) Side view with an inset of the bubble at maximum expansion in the first frame. When the needle jet (NJ) is generated, a shock wave ("SW") is emitted and gets partly reflected at the bubble interface (rSW). (b) Magnified view of the region where the needle jet is formed. The dashed horizontal line depicts the boundary. (c) Bottom view through a transparent boundary and illumination from the top. The three rows are consecutive of three experiments with $\gamma = 0.053 \pm 0.021$, maximum radii $R_{max} = 733\,\mu$m, $R_{max} = 690\,\mu$m and $R_{max} = 580\,\mu$m for (a), (b), and (c), respectively.

may be even higher as we have assumed that the flow reaches v_{NJ} within half the frame interval time of 200 ns. The apparent radius of the needle jet, observed through the curved bubble wall, is less than 12.5 μm.

Let us now discuss in more detail the experimental results shown in Fig. 3. In the first frame of Fig. 3(b), the closing of the bubble neck by the kink protruding toward the axis of symmetry can be observed. From tracking the displacement of the bubble wall at the closing neck over subsequent frames, we can obtain the corresponding velocity of this flow. It increases from about 50 ms^{-1} at $\tilde{t} = -1.5\,\mu$s to 250 ms^{-1} at $\tilde{t} = 0.1\,\mu$s, relative to the time of impact of the flow on the axis of symmetry, $\tilde{t} = 0$. In the third frame of Figs. 3(a) and 3(b), this flow collides on the axis, thereby creating a shock wave into the liquid phase and the needle jet ("NJ") into the gas phase. We consider the instance of shock emission as the moment of needle jet formation. The shock front has propagated spherically outward and is trailed by a second pressure transient that is likely a reflection of the primary shock wave from the bubble's liquid–gas interface. It has a reversed intensity step, which implies a pressure phase shift of roughly π from the sound soft bubble interface. This wave is labeled "rSW." The origin of shock wave emission is indicated by the "x" in the previous frame in row (a). It is the center of a circle fitted to the shock front. It lies close to the axis where the neck is the thinnest, and the cylindrical flow collides. There, it may also meet with the axial flow from above that would form the regular jet. In the fourth frame, the needle jet has traversed the bubble and impacted onto the boundary. Note that the bubble is mirrored by the metallic surface. The needle jet is clearly visible within the bubble due to a mildly diffusive back-illumination [see (a) and (b)]. It reveals a rather complex and fragmented shape. We speculate that this is due to the impact and subsequent splashing and depicts the atomization of the needle jet. Therefore, high-speed droplets are formed, some of them impacting with the gas–liquid interface moving downwards. A careful look on this interface in the last frame reveals undulations [see the arrow in Fig. 3(b)] that we interpret as a result of the impact of droplets. The atomization of the needle jet is particularly visible in the view through the boundary in Fig. 3(c). For this, the metallic boundary has been replaced with a slab of glass. Here, the scene is illuminated from the liquid side, resulting in the outer dark ring from the peripheral bubble interface that is almost perpendicular to the boundary. The camera focus is set to provide a sharp image of the surface of the glass. The image of the central cap with a bright inner region is indicated with an arrow in the first frame. The neck between the caps closes and collapses in this sequence between the third and the fourth frame. In the fourth frame of Fig. 3(c), the needle jet has already impacted onto the boundary. It is the central region that has changed from bright in frame three to dark in frame four. The fifth frame depicts besides the dark central region spherical objects out of focus that we identify with droplet impacts from the splashing needle jet.

From the experimental recordings, it is evident that the needle jet forms once the liquid collides onto the gas column of the neck. For this event, we derive a simplified flow model to demonstrate the principle of the needle jet formation. While the calculation of the precise bubble dynamics is important to obtain a convergent radial flow, a needle jet should always form when a convergent flow meets with a slender gas volume present along the axis of symmetry. Figure 4 (top

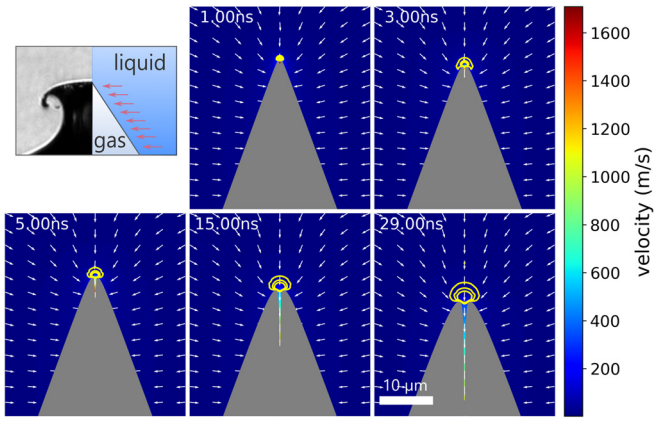

FIG. 4. Simplified computational model of the converging flow in the neck region, which results in the needle jet as well as flow fields and pressure contours (in yellow) of the numerical results of needle jet generation. The arrows indicate the direction, and the color the magnitude of the flow.

left) shows the axisymmetric domain of our model. We assume a cylindrically convergent flow around a slender gas volume and use the incompressible solver Gerris[22] based on the Volume of Fluid method. It accounts for viscous and interfacial tension between water and air, see the supplementary material for more details. In Fig. 4, the resulting flow fields and pressure contours show the formation of a high-pressure region (yellow lines) on the tip of the gaseous cone. There, the radial inward flow is accelerated and shoots similar to that in the experiment a surprisingly thin jet into the gaseous cone. Still, two open questions remain, concerning which maximum speed may potentially be reached by this singularity and which physical properties are the relevant limiting factors. Our experiments give a lower boundary of the average needle-jet velocity of 850 ms^{-1}, Lechner *et al.* 2019[15] obtain in their simulations velocities above 1300 ms^{-1}, while our simulations yield a maximum velocity of over 2000 ms^{-1}. Probably for this inertia dominated dynamics, viscosity and compressibility (see the shock wave radiation at needle jet generation) have to be taken into account.

Flow focusing into a gas phase resulting in filamentary high-speed jetting, in general,[8] has also been observed in other axisymmetric convergent flows. For example, an axial so-called Worthington jet can be produced from the singularity produced by a closing liquid crater.[3,9,28] Michon *et al.*[17] produced craters by drops impacting on a liquid pool such that at the bottom of the closing crater, where capillary waves meet and form a dimple, thin jets can be generated. In their configuration, viscosity seems to play a twofold role, as expected it limits the jet velocity but, on the other hand, it also stabilizes the closing crater geometry that is necessary for generation of the fine jets. The fastest jets are produced when the crater does not pinch off (split) during its closure but closes in a geometry similar to our model in Fig. 4, see also Ref. 26. Zeff *et al.*[30] produced a flow singularity with super-critical Faraday waves. They make a potential flow description and tackle the singularity with a similarity method. Also buoyant, rising bubbles when they reach the liquid surface can produce jetting through a similar flow singularity.[7] In those configurations, driving forces are surface tension and sometimes buoyancy, resulting in flow velocities of tens of meters per second and thus much smaller than in our work of cavitation bubbles where the dynamics are inertia dominated.

High speed jetting in a splitting, elongated bubble further away from an elastic boundary has previously been communicated. Brujan *et al.*[6] report jet velocities of approximately 800 ms^{-1}, which they estimated from the deformation of their bubble shadowgraph. Eventually, the jet impacted with a velocity of up to 170 ms^{-1} onto the boundary. Another geometry leading to bubble elongation and splitting that results in fast jets is through the confinement in a thin liquid gap, e.g., Zeng *et al.*[31] While for elongated, splitting bubbles typically two oppositely directed jets are formed, in the present study, a single jet is generated and focused onto the boundary at high speeds.

Considering the high increase in velocities achieved from the cylindrically convergent geometry in general, it comes to no surprise that this type of flow focusing is also technically applied where violent hydrodynamics are involved. This is, for example, the case, where hard material has to be pierced and is used by shaped charges and lined cavities in mining or even for bazookas.[5] These applications rely on similar cylindrical convergence in order to accelerate a liquid jet.

Finally, we investigate at which stand-offs the needle jet is formed. We identify three phenomena that characterize the respective bubble dynamics: (I) the formation of the needle jet itself, accompanied by a shock wave, (II) the formation of the cylindrically convergent flow, resulting in the circumferential kink, and (III) the formation of the regular jet threading the intact bubble. In Fig. 5, five shapes of cavitation bubbles shortly before their jet impact on the boundary are shown. We find for all $\gamma < 0.17$ the formation of the supersonic needle jet. Then, the kink is so pronounced as to produce the neck and bubble cap. In contrast for $\gamma > 0.23$, the well-known and slower regular jet is formed. This largely confirms the numerical prediction by Lechner *et al.*[16] who found a similar value for this threshold. The kink is observed for $\gamma < 0.68$. Comparison between the shapes reveals a competition between the cylindrical, converging flow leading to the needle jet and the axial flow developing into the regular jet. The needle-jet formation is hindered once the regular jet drags the gas column such that the convergent cylindrical flow does not occur near the gas phase. As for decreasing stand-off, the regular jet becomes slower and develops somewhat later during the bubble collapse,[16,20] the needle-jet is only found for the smallest stand-offs. In the interval

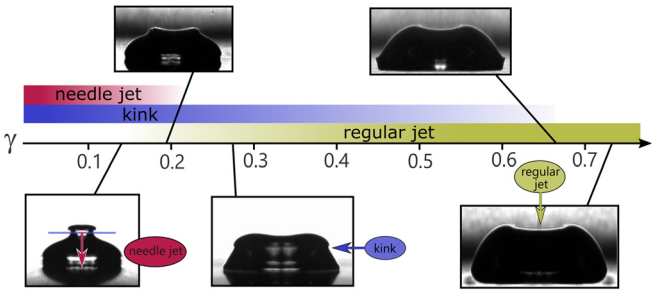

FIG. 5. Illustration of stand-off regimes with either regular or needle jetting and occurrence of the kink. For more opaque colors along the horizontal bars, the respective phenomenon appears more pronounced. Bubble shapes are taken shortly before jet impact on the solid. Only the bubble at the smallest stand-off generates the needle-jet. The other bubbles are all indented by the regular jet. For increasing stand-off, the kink is less pronounced and closer to the boundary. For the largest stand-off where still a kink appears ($\gamma = 0.67$), it seems degenerate being produced directly at the boundary, while at $\gamma = 0.73$, there is no kink at all.

$0.17 < \gamma < 0.68$, a kink is formed and we observe that the cylindrical flows associated with it merge and amplify the regular jet. In the lower transition regime $0.17 < \gamma < 0.23$, the convergent flow and the regular jet tend to meet on the axis of symmetry approximately at the same time. Here, sometimes a needle jet may still be formed, but, in general, we observe a complex three-dimensional flow pattern. We also want to note that the bubble dynamics at the boundary is visibly affected by the liquids viscosity. As, however, the definition of γ does not incorporate the viscosity, the stated γ-values are strictly valid only for water and $R_{max} \approx 600\,\mu$m.

In summary, we report the transformation of a cavitation bubble into a micrometer-sized, supersonic needle jet with an averaged velocity of more than 850 ms^{-1}. It is the first photographic proof of this needle jet and its supersonic velocity predicted by axisymmetric simulations.[15] It turned out that asymmetries inherently present to experiments do not prevent the focusing of a planar convergent flow to the axis symmetry. Once this flow impacts on and near a slender gaseous cavity, a needle jet is formed. We want to emphasize that the formation mechanisms behind the needle-jet and the regular jet are very distinct. The needle jet is only observed when the cylindrically flow converges on the axis of symmetry with a slender gas body being present. This mechanism resembles the one reported in a few numerical works concerning elliptical bubbles more distant from a boundary.[1,27] The impact pressure or water hammer pressure of the regular jet on a solid is frequently discussed and connected with cavitation erosion. The water hammer pressure expected from the needle jet is one order of magnitude larger than the ones of the regular jet and the stagnation pressures, being quadratic in the jet velocity, even a hundred-fold larger than that of the regular jet. Thus, the needle jet may play a role in cavitation erosion not noticed before. The finding of this supersonic needle-jet at this small stand-off regime has further direct implications for surface processing with single, laser-induced bubbles, such as laser-based peening,[25] laser ablation in liquids (LAL) for nanoparticle generation,[2,10] or laser surgery. In general, the relative ease by which the needle-jet is generated at a precisely controllable location may offer approaches for targeted material processing as well as for drug delivery in medicine and biology. There, the needle jet could perforate a tissue layer and the following regular jet could inject a larger liquid volume.

See the supplementary material for technical details on the jet velocity measurements and on the numerical simulations.

This research was funded by the Deutsche Forschungsgemeinschaft (DFG, German Research Foundation) under grant OH 75/4-1.

DATA AVAILABILITY

The data that support the findings of this study are available within the article and its supplementary material.

REFERENCES

[1]A. A. Aganin, L. A. Kosolapova, and V. G. Malakhov, "Dynamics of a spheroidal gas bubble near a rigid surface," J. Phys. **1328**, 012043 (2019).
[2]S. Barcikowski, A. Plech, K. S. Suslick, and A. Vogel, "Materials synthesis in a bubble," MRS Bull. **44**(5), 382–391 (2019).
[3]D. Bartolo, C. Josserand, and D. Bonn, "Singular jets and bubbles in drop impact," Phys. Rev. Lett. **96**(12), 124501 (2006).
[4]T. B. Benjamin and A. T. Ellis, "The collapse of cavitation bubbles and the pressures thereby produced against solid boundaries," Philos. Trans. R. Soc. London, Ser. A **260**, 221–240 (1966).
[5]G. Birkhoff, D. P. MacDougall, E. M. Pugh, and S. G. Taylor, "Explosives with lined cavities," J. Appl. Phys. **19**(6), 563–582 (1948).
[6]E.-A. Brujan, K. Nahen, P. Schmidt, and A. Vogel, "Dynamics of laser-induced cavitation bubbles near an elastic boundary," J. Fluid Mech. **433**(1), 251–281 (2001).
[7]L. Deike, E. Ghabache, G. Liger-Belair, A. K. Das, S. Zaleski, S. Popinet, and T. Séon, "Dynamics of jets produced by bursting bubbles," Phys. Rev. Fluids **3**(1), 013603 (2018).
[8]J. Eggers and E. Villermaux, "Physics of liquid jets," Rep. Prog. Phys. **71**(3), 036601 (2008).
[9]S. Gekle and J. M. Gordillo, "Generation and breakup of worthington jets after cavity collapse. Part 1. Jet formation," J. Fluid Mech. **663**, 293 (2010).
[10]S. Ibrahimkutty, P. Wagener, A. Menzel, A. Plech, and S. Barcikowski, "Nanoparticle formation in a cavitation bubble after pulsed laser ablation in liquid studied with high time resolution small angle x-ray scattering," Appl. Phys. Lett. **101**(10), 103104 (2012).
[11]M. Jalaal, S. Li, M. Klein Schaarsberg, Y. Qin, and D. Lohse, "Destructive mechanisms in laser induced forward transfer," Appl. Phys. Lett. **114**(21), 213703 (2019).
[12]K. Ki-Han, C. Georges, F. Jean-Pierre, and K. Ayat, *Advanced Experimental and Numerical Techniques for Cavitation Erosion Prediction* (Springer, 2014), Vol. 106.
[13]W. Lauterborn and H. Bolle, "Experimental investigations of cavitation-bubble collapse in the neighbourhood of a solid boundary," J. Fluid Mech. **72**(2), 391–399 (1975).
[14]W. Lauterborn and T. Kurz, "Physics of bubble oscillations," Rep. Prog. Phys. **73**(10), 106501 (2010).
[15]C. Lechner, W. Lauterborn, M. Koch, and R. Mettin, "Fast, thin jets from bubbles expanding and collapsing in extreme vicinity to a solid boundary: A numerical study," Phys. Rev. Fluids **4**(2), 021601 (2019).
[16]C. Lechner, W. Lauterborn, M. Koch, and R. Mettin, "Jet formation from bubbles near a solid boundary in a compressible liquid: Numerical study of distance dependence," Phys. Rev. Fluids **5**(9), 093604 (2020).
[17]G.-J. Michon, C. Josserand, and T. Séon, "Jet dynamics post drop impact on a deep pool," Phys. Rev. Fluids **2**(2), 023601 (2017).
[18]C.-D. Ohl, M. Arora, R. Dijkink, V. Janve, and D. Lohse, "Surface cleaning from laser-induced cavitation bubbles," Appl. Phys. Lett. **89**(7), 074102 (2006).
[19]A. Patrascioiu, C. Florian, J. M. Fernández-Pradas, J. L. Morenza, G. Hennig, P. Delaporte, and P. Serra, "Interaction between jets during laser-induced forward transfer," Appl. Phys. Lett. **105**(1), 014101 (2014).
[20]A. Pearson, J. R. Blake, and S. R. Otto, "Jets in bubbles," J. Eng. Math. **48**(3-4), 391–412 (2004).
[21]A. Philipp and W. Lauterborn, "Cavitation erosion by single laser-produced bubbles," J. Fluid Mech. **361**, 75–116 (1998).
[22]S. Popinet, "Gerris: A tree-based adaptive solver for the incompressible Euler equations in complex geometries," J. Comput. Phys. **190**(2), 572–600 (2003).
[23]F. Reuter and R. Mettin, "Mechanisms of single bubble cleaning," Ultrason. Sonochem. **29**, 550–562 (2016).
[24]P. Serra and A. Piqué, "Laser-induced forward transfer: Fundamentals and applications," Adv. Mater. Technol. **4**(1), 1800099 (2019).
[25]H. Soyama, "Cavitation peening: A review," Metals **10**(2), 270 (2020).
[26]S. T. Thoroddsen, K. Takehara, H. D. Nguyen, and T. G. Etoh, "Singular jets during the collapse of drop-impact craters," J. Fluid Mech. **848**, 2018 (2018).
[27]O. V. Voinov and V. V. Voinov, "On the pattern of cavitation bubble collapse near the wall and formation of cumulative jet," Dokl. Akad. Nauk **227**, 63–66 (1976).
[28]K. Yamamoto, M. Motosuke, and S. Ogata, "Initiation of the Worthington jet on the droplet impact," Appl. Phys. Lett. **112**(9), 093701 (2018).
[29]J. Yan, Y. Huang, C. Xu, and D. B. Chrisey, "Effects of fluid properties and laser fluence on jet formation during laser direct writing of glycerol solution," J. Appl. Phys. **112**(8), 083105 (2012).
[30]B. W. Zeff, B. Kleber, J. Fineberg, and D. P. Lathrop, "Singularity dynamics in curvature collapse and jet eruption on a fluid surface," Nature **403**(6768), 401–404 (2000).
[31]Q. Zeng, S. R. Gonzalez-Avila, and O. Claus-Dieter, "Splitting and jetting of cavitation bubbles in thin gaps," J. Fluid Mech. **896**, A28 (2020).